Biomaterials Science

ROYAL SOCIETY OF CHEMISTRY

PAPER

View Article Online
View Journal | View Issue

Cite this: *Biomater. Sci.*, 2022, **10**, 1304

Treatment of kidney clear cell carcinoma, lung adenocarcinoma and glioblastoma cell lines with hydrogels made of DNA nanostars†

Manuela Leo, [a] Enrico Lattuada, [a] Debora Caprara, [a] Luisa Salvatori, [b] Andrea Vecchione, [c] Francesco Sciortino, [a] Patrizia Filetici [b] and Antonella Stoppacciaro *[c]

Received 26th October 2021,
Accepted 22nd December 2021

DOI: 10.1039/d1bm01643a

rsc.li/biomaterials-science

Overcoming the systemic administration of chemotherapy to reduce drug toxicity and the application of personalised medicine are two of the major challenges in the treatment of cancer. To this aim, efforts are focused on finding novel nanomaterials for the targeted administration of drugs and bioactive molecules in the tumor sites. DNA-based hydrogels are promising candidates for these applications. However, while such materials are fairly known from a structural and physical standpoint, their effects on cell cultures are far less investigated. Here, we studied the biological response of three different cell lines (clear cell renal cell carcinoma 786-O, lung adenocarcinoma H1975 and glioblastoma U87MG) to the treatment with DNA-GEL – a DNA-based hydrogel composed of interacting DNA nanostars. Additionally, we investigated the structural modification of DNA-GELs under cell culture conditions. The results we collected show a cell type specificity of the response, with interesting implications for future applications.

1. Introduction

DNA – the strip holding the codified genetic information of living organisms – can be successfully used as a brick to build biocompatible materials, thus representing an innovative tool for applications in therapy and biomedicine. The self-assembly of properly designed three-dimensional DNA nanostructures leads to the formation of supramolecular aggregates, which become the fundamental building blocks of new generation DNA materials.

Starting from Seeman's idealized models of colloidal particles,[1] it is possible to realize DNA hydrogels composed of DNA nanostars (NSs).[2,3] These DNA nanostructures have multiple arms departing from a common central junction (whose number can be tuned at the design time), which can interact through the hybridization of single DNA strands placed on the tips of the arms. Due to the reversibility and temperature dependence of the DNA interactions, the gel formation is mainly controlled by the temperature. Therefore, DNA hydrogels can be repeatedly melt and formed at high and low temperatures, respectively. However, DNA NSs can be purposely designed in order to obtain gels with different behaviours and stimuli-responsive properties. Some examples were reviewed by Lattuada *et al.*,[3] from gels composed of simple interacting NSs[2,4] to more sophisticated ones, such as the re-entrant DNA gels, which are able to form within specific temperature ranges and behave as a liquid at higher and lower temperatures.[5]

Selected DNA hydrogels have been successfully used in immunotherapy[6–10] and for the delivery of small molecules.[6–8,11–16] Despite these far-reaching applications, very little is known about how cells respond to these materials and, *viceversa*, how these materials respond to the cell culture conditions. For instance, is any molecular mechanism activated by the presence of DNA gels? what is the structure acquired by the network formed by the DNA NSs in conditions of culture media and biological fluids? The latter is important from a biological standpoint, because it constitutes the real substrate applied to cells in cultures. In fact, we can expect the macrostructure of DNA hydrogels to change with the temperature and the composition of the growth medium.[2,5,17]

Here, we investigated the response of three different cell lines – clear cell renal cell carcinoma 786-O, non-small cell lung adenocarcinoma H1975 and glioblastoma U87MG – to treatment with suspensions of DNA-GEL and DNA-NoGEL,

[a]*Department of Physics, Sapienza University of Rome, Piazzale Aldo Moro 5, 00185 Rome, Italy*
[b]*Institute of Molecular Biology and Pathology, National Research Council, c/o Sapienza University of Rome, Piazzale Aldo Moro 5, 00185 Rome, Italy*
[c]*Department of Clinical and Molecular Medicine, Sapienza University of Rome, St. Andrea Hospital, Via di Grottarossa 1035, 00189 Rome, Italy.*
E-mail: antonella.stoppacciaro@uniroma1.it

†Electronic supplementary information (ESI) available. See DOI: 10.1039/d1bm01643a

which do and do not form a DNA hydrogel, respectively. The DNA NSs forming both suspensions are similar to the ones investigated by Biffi *et al.*[2] The NSs constituting the DNA-GEL were designed to interact *via* the hybridization of the sticky ends on the arm tip to form a gel at the human body temperature ($T \simeq 37$ °C). In the DNA-NoGEL design, the sticky ends were removed, so that the NSs are not able to bind and form a network (*i.e.*, the suspension always remains in a "fluid" state). The cell lines were treated in time with DNA-GEL and DNA-NoGEL and we observed the response in terms of proliferation, cell cycle progression and migration ability. We also investigated the behaviour of DNA-GEL and DNA-NoGEL under cell culture conditions and their response to the presence of proteins.

Our results show that specific cell lines display a different response to DNA-GEL treatment, the most notable being the block of proliferation induced by DNA-GEL treatment on the glioblastoma U87MG cell line. Furthermore, we found that the typical sponge-like structure of DNA hydrogels – where regions with a higher concentration of NSs alternate with more dilute regions – is modified not only by the temperature but also by the presence of proteins.

To the best of our knowledge, this is the first study that characterizes the effects of DNA gels on different cell lines in parallel. Collecting information regarding the response of selected cell lines to DNA-GEL will certainly contribute to set up future protocols for the delivery of drugs and/or nucleic acids in targeted tissues. This might represent, in fact, an efficient tool for the targeted application of concentrated bioactive molecules on site, providing a novel way for the delivery of bioactive molecules inside the tissues or to induce a slow diffusion of drugs and molecules *in situ*, thus avoiding detrimental systemic drug administration. From this perspective, the change of the DNA-GEL macrostructure might be used for purposely choosing the gel features according to the experimental/therapeutic requirements, in order to obtain the delivery of specific molecules, proteins or antibodies. Finally, DNA hydrogels could be particularly useful in tissues that are difficult to access like the brain: in particular, it will be a challenge to understand and study the response to the treatment of glioblastoma – a tumor known to be unresponsive to antiproliferative drugs.[18]

2. Materials and methods

2.1. NS system

We experimentally realized bulk quantities of DNA tetravalent NSs composed of four double-stranded arms of 20 base pairs. A core of eight unpaired thymines provides structural flexibility to the NS. In the case of the NSs forming the DNA-GEL, each arm terminates with an 8-base self-complementary sticky sequence, which allows the NS–NS interaction. Before each sticky sequence, an extra adenine is inserted to favour the sticky-end flexibility and the linking between NSs.

The DNA sequences used to produce the DNA NSs were purchased from Integrated DNA Technologies with standard desalting purification and used without any further treatment. The sequences we used for the experiments, inspired by the ones used by Biffi *et al.*,[2] are listed below:

5'-CTACTATGGCGGGTGATAAA TT CGGGAAGAGCATGCCCATCC (A GCGTACGC)-3'
5'-GGATGGGCATGCTCTTCCCG TT CTCAACTGCCTGGTGATACG (A GCGTACGC)-3'
5'-CGTATCACCAGGCAGTTGAG TT CATGCGAGGGTCCAATACCG (A GCGTACGC)-3'
5'-CGGTATTGGACCCTCGCATG TT TTTATCACCCGCCATAGTAG (A GCGTACGC)-3'.

The complementary sequences forming the NS arms are highlighted with the same colors. The sticky-end sequences, which are present in the DNA NSs forming the DNA-GEL only, are highlighted in parentheses.

Fluorescent DNA NSs were obtained by modifying one of the four DNA sequences. Specifically, one of the thymines constituting the NS core was conjugated with a fluorescein isothiocyanate molecule (FITC):

5'-CTACTATGGCGGGTGATAAA T-[FITC]T
CGGGAAGAGCATGCCCATCC (A GCGTACGC)-3'.

Again, the sticky-end sequence of the DNA NSs forming the DNA-GEL is highlighted in parentheses.

These oligonucleotides were designed to hybridize into star-shaped structures with four arms at around $T_{NS} \approx 65$ °C *via* the Watson–Crick pairing.[2] The different lengths of the arms and sticky overhangs allow the self-assembly of the NSs to occur at a temperature well above that for the binding between different NSs. For both systems, at a very high temperature (*i.e.*, for $T > T_{NS}$), the system consists a suspension of freely diffusing DNA single strands. By slowly lowering T, the complementary strands start to self-assemble, so that, for $T < T_{NS}$ (or $T_g < T < T_{NS}$ for the DNA-GEL samples, where T_g is the gel-formation temperature), the system is composed of weakly interacting tetravalent NSs.

In the case of DNA-GEL, the system displays a two-state temperature behaviour: on further cooling, for $T < T_g$, the NSs progressively bind *via* the sticky-end sequences, giving rise to a spanning network of bonded particles. The temperature behaviour of the NSs is represented in Fig. 1.

2.2. Phase diagram estimation

The phase diagram of the DNA-GEL system – though for a different sticky-end sequence and solvent ionic strength – was studied in the past by some of the authors[2] (see Fig. 2A, black symbols). When the sample is prepared with a concentration within the range of the consolution curve ($15 \lesssim c \lesssim 280$ μM), for $T < T_{ps}$, it phase separates into NS-poor and NS-rich phases. The latter can be considered as a gel prepared at the (larger) concentration of the NS-rich branch of the coexisting

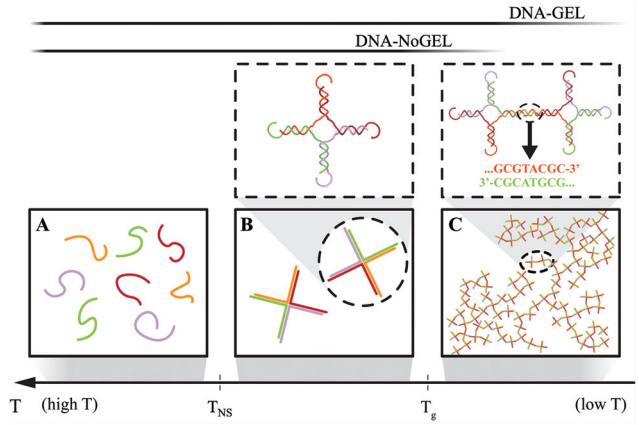

Fig. 1 Temperature behaviour of the NS. (A) For $T > T_{NS}$, the strands do not self-assemble and are free to diffuse. (B) For $T < T_{NS}$, the strands form star-shaped structures which weakly interact. (C) For $T < T_g$, in the DNA-GEL system only, the NSs progressively bind, forming a spanning network. The top panels, from left to right, show the NS structure and the binding of two NSs, respectively.

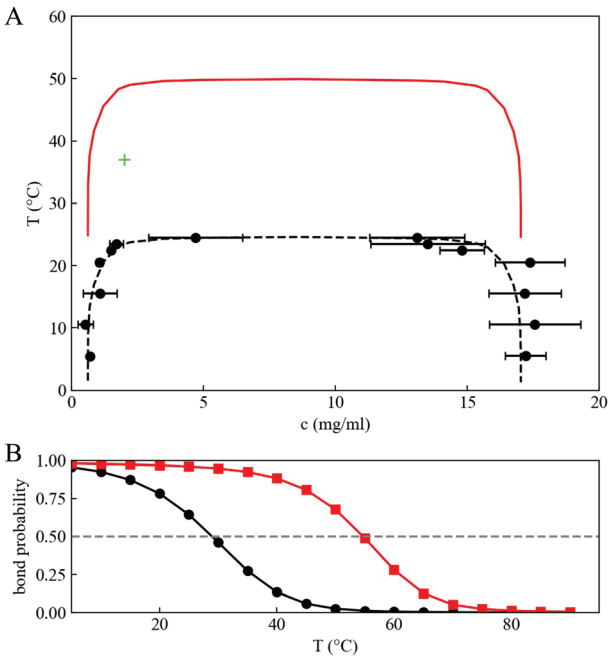

Fig. 2 (A) Phase diagram of the DNA-GEL system. The black dots (data from Biffi *et al.*[2]) show the experimentally determined consolution curve for the same DNA NSs used here but with a different sticky-end sequence (*CGATCG*), suspended in 50 mM NaCl. The black dashed line is drawn to guide the eye. The red curve is the estimated consolution curve for the DNA-GEL NSs used in the present work in 115 mM NaCl. The green plus symbol indicates the experimental conditions (c = 35 μM, T = 37 °C). (B) Bond probability of the sticky-end sequences computed under the different working conditions: the *CGATCG* sticky-end in 50 mM NaCl solvent, used in Biffi *et al.*[2] (black circles) and the *GCGATCGC* sticky-end sequence used in this work in 115 mM NaCl solvent (red squares). The open triangles on the horizontal axis indicate the temperature corresponding to a 50% fraction of the bonded bases for the two sticky ends. Colors are the same as those of (A).

line. The former, conversely, is akin to dilute dispersion (gas) of NSs. The precise determination of the phase separation region for the NSs used in the experiments reported here would require long and painstaking measurements of the concentrations of the two phases forming at the different temperatures and solvent conditions used, which is not the aim of the present work. We can, however, obtain an estimate of the phase separation region boundary, at least in the most simple case, by exploiting the principle of extended corresponding states,[19,20] which allows to map two systems interacting *via* short-range potentials one onto the other. For colloids with strongly directional interactions (*i.e.*, for patchy particles), which is the theoretical model closer to the DNA NSs, it was demonstrated[20] that the locus of the critical point only depends on the geometry of the attractive spots and on the bond probability. This observation is consistent with Wertheim's theory,[21,22] predicting that systems with different attraction strengths (but same hard-core and same number of patches) are described by the same thermodynamic potentials when expressed as a function of particle density and binding probability. Since the size and the geometry of the NSs used here do not change from the ones used in Biffi *et al.*[2] and the length of the sticky ends is very similar in the two cases, we can assume that the concentration dependence of the phase coexistence boundary does not appreciably change. The temperature, instead, strongly depends on the bond probability, which in turn depends on the number of nucleobases in the sticky sequence (at least for short sequences). In this work, we assume that: (a) the concentration of the two phases which form does not change appreciably from the system of Biffi *et al.*,[2] which we take as a reference, and (b) that the bond probability of the sticky tips is a good parameter for the phase separation of the system. With these assumptions, the new consolution curve is then computed as:

$$T'(c) = T(c)\frac{T_{50}}{T_{50}^{\mathrm{ref}}}, \qquad (1)$$

where T_{50} and T_{50}^{ref} are the temperatures (in Kelvin) corresponding to a 50% bond probability for the experimental and reference NS systems, respectively. Fig. 2B shows the temperature dependence of the bond probability of the sticky-end sequence used in Biffi *et al.*[2] (*CGATCG* in NaCl, 50 mM), along with the one used in this work (*GCGATCGC* in NaCl, 115 mM), evaluated *via* the hybridization of free energies[23] implemented using the package NUPACK.[24] In Fig. 2A, we show the consolution curve evaluated using eqn (1). In the same figure, we also highlight the experimental conditions used throughout this work: c = 35 μM and T = 37 °C.

2.3. DNA-GEL and DNA-NoGEL preparation

Stock solutions of DNA-GEL and DNA-NoGEL, 274 μM, were obtained by first reconstituting the distinct lyophilized oligonucleotides constituting the DNA NSs and then dissolving equimolar quantities of the single reconstituted DNA strands in 50 mM NaCl solution. The NS annealing was performed by

heating the batches at T = 95 °C for 20 min and then by slowly cooling down the temperature to T = 25 °C.

The samples used for the experiments were prepared by first heating up the stock solutions at T = 65 °C for 5 min to unbind the links between the DNA NSs and then by mixing the solutions with DNAse/RNAse-free Milli-Q water at the same temperature. The solutions were then homogenized using a vortex mixer. Finally, the samples were dissolved in a 2× cell culture medium DMEM/Ham's F12 mixture (Sigma-Aldrich) to obtain a solution of NSs at a concentration c = 35 μM.

2.4. Fluorescence microscopy and DNA-GEL characterization

DNA-GEL and DNA-NoGEL samples for fluorescence microscopy were obtained by mixing FITC-conjugated DNA NSs with the unconjugated ones at a ratio of 1 : 200. Bovine Serum Albumin (BSA) conjugated with Texas Red™ (Thermo Fisher Scientific) was mixed with unconjugated BSA at a ratio of 1 : 50.

Samples were prepared by first heating DNA-GEL and DNA-NoGEL batches at T = 65 °C for 5 min. Then, an appropriate amount of solution to obtain a final NS concentration of c = 35 μM was mixed:

• with DMEM cell culture medium supplemented (DMEM-FBS) or not with 10% Fetal Bovine Serum (FBS) or

• with 116 mM NaCl solution not containing or containing BSA in different amounts (2.5 μg μl^{-1}; 1 μg μl^{-1}; and 0.5 μg μl^{-1}), 10% FBS (2.5 μg μl^{-1} in proteins), fibronectin (1 μg μl^{-1}), or Matrigel (2.5 μg μl^{-1}).

Each sample was homogenized using a vortex mixer, deposited in a 35 mm Petri dish and incubated in a humidified chamber at T = 37 °C for 24 or 48 h. Fluorescence was visualized using a Nikon Eclipse 90i microscope equipped with a QICAM Fast 1394 Digital Camera (QImaging).

The size of the pores was estimated from the fluorescence images by computing the image normalized autocorrelation function:

$$\mathrm{corr}(u,v) = \frac{\sum_{x,y}[I(x,y)-\bar{I}][J(x-u,y-v)-\bar{J}]}{\sqrt{\sum_{x,y}[I(x,y)-\bar{I}]^2 \sum_{x,y}[J(x-u,y-v)-\bar{J}]^2}}, \quad (2)$$

where $\bar{I}$ ($\bar{J}$) is the average of the image (template) in the overlap region and the sum is evaluated for the pixels in the overlap region. The normalized autocorrelation function was computed using the *normxcorr2* function of Matlab. The formula quantifies the self-similarity of an image with a shifted (by (u, v)) version of itself. Finally, the normalized autocorrelation function is radially averaged around the origin. The average pore size ξ is conveniently defined as the radial distance corresponding to a value of 0.5 of the normalized autocorrelation function.

2.5. Cell lines and the proliferation assay

Clear cell renal cell carcinoma 786-O, non-small cell lung adenocarcinoma H1975 and glioblastoma U87MG human cell lines (obtained from the American Type Culture Collection, Manassas, VA, USA) were grown at T = 37 °C under a humidified atmosphere of 5% CO_2 in DMEM/Ham's F12 mixture (Sigma-Aldrich), supplemented with FBS 10% (Sigma-Aldrich), 2 mM L-glutamine, 25 U ml^{-1} penicillin and 25 U ml^{-1} streptomycin (Biowest). For the cell culture experiments, cells were seeded 24 h before treatment and then the medium was replaced with a fresh complete DMEM/Ham's F12 mixture containing or not containing DNA-GEL and DNA-NoGEL (c = 35 μM) prepared as described above. Cell proliferation and viability were evaluated after 24, 48 and 72 h of incubation. Cells were collected after trypsinization, stained with Trypan Blue (0.04%, Gibco) and vital cells were counted in a Burker chamber. Alternatively, cells were incubated for 48 h with or without DNA-GEL and DNA-NoGEL, and then washed three times with PBS (Lonza) to remove the DNA NSs and incubated again with a fresh complete DMEM/Ham's F12 mixture and counted at the indicated time intervals.

2.6. Western blot analysis

Cells were seeded 24 h before incubation and then the medium was replaced with a DMEM/Ham's F12 mixture containing or not containing DNA-GEL and DNA-NoGEL (c = 35 μM). Cells were collected after 24 and 48 h of incubation, resuspended in Laemmli buffer and heated for 5 min at T = 90 °C. Protein extracts were run on 10% SDS-PAGE, blotted onto nitrocellulose (Amersham) and hybridized with anti-Cyclin D1 (Dako), anti-Cyclin A, anti-CDC25c, anti-Bcl2 and anti-GAPDH (Santa-Cruz) antibodies. Protein signals were detected using a SuperSignal West Dura Extended Duration Substrate (Thermo Scientific), visualized using a ChemiDoc™ MP Imaging System (Bio-Rad) and quantified using ImageLab analysis software.

2.7. Immunofluorescence analysis

Cells were seeded on a glass coverslip inside a 35 mm Petri dish 24 h before the treatment and then the medium was replaced with a fresh complete DMEM/Ham's F12 mixture containing or not containing fluorescent DNA-GEL and DNA-NoGEL (c = 35 μM; 1 : 3 ratio of FITC-conjugated and unconjugated DNA NSs). Samples were collected at different times (0, 24, 48 and 72 h) and immunofluorescence was performed as follows. Cells were washed three times with PBS and fixed with 90% EtOH plus 0.4% paraformaldehyde for 15 min, permeabilized with 0.3% Triton X-100 (Sigma-Aldrich) for 5 min and blocked with blocking buffer (PBS plus 3% BSA and 0.1% Tween) for 1 h. Then, the cells were incubated overnight with anti-CD147 (Abcam), washed three times with blocking buffer and incubated again with the anti-Rabbit TRITC-conjugated antibody (Thermo Fisher Scientific) for 1 h. Finally, the cell nuclei were stained with 4′,6-diamidino-2-phenylindole (DAPI, Calbiochem). Images of the samples were acquired using a Nikon Eclipse 90i fluorescence microscope equipped with a QICAM Fast 1394 Digital Camera.

2.8. Scratch test and single cell tracking

Cell migration was evaluated by a wound healing assay.[25] The cells were seeded in a 96-well plate and cultured until confluence and then the medium was replaced with a fresh complete

DMEM/Ham's F12 mixture containing or not containing DNA-GEL and DNA-NoGEL (c = 35 μM). After 24 h of incubation, the cell samples were wounded using a 200 μl pipette tip. Images of the scratched regions were acquired every 24 h for several days using an inverted Nikon Eclipse TE2000-S microscope. For the cell migration experiments after the removal of DNA, cells were treated for 48 h with a complete DMEM/Ham's F12 mixture containing or not containing DNA-GEL and DNA-NoGEL (c = 35 μM), and then washed three times with PBS and incubated with a fresh complete DMEM/Ham's F12 mixture. The scratch was made after 24 h and the images were acquired for several days. The cell-filled area was measured after 48 h using the ImageJ MRI Wound Healing Assay tool. Data are shown as mean ± SEM (standard error of means) of two independent experiments.

Additionally, time-lapse videos of the scratch regions on the samples were acquired after about 30 min from the scratch. The images were taken at a fixed frame rate, every Δt = 180 s, using a CMOS camera (Basler acA2040-120um) with an effective pixel size of $\Delta x \approx 1.9$ μm per pixel. The motion of the single cells was measured from the images using the TrackMate plugin of ImageJ.[26] The mean square displacement (MSD) of the cells was computed from their tracked positions as

$$\mathrm{MSD}(t) = \frac{1}{N}\sum_{i=1}^{N} |r_i(t) - r_i(0)|^2, \qquad (3)$$

where N is the number of cells detected in the image and $r_i(t)$ is the (x,y) position of the i-th cell at time t. All the analyses were performed on a region near the wound. No significant drift was observed for all the time-lapse videos collected.

2.9. Statistical analysis

All data are given as mean ± SEM (standard error of mean) of at least three independent experiments, unless differently stated. For determining the statistical significance, Student's t-test was performed; p-value ≤0.05 (*), p-value ≤0.01 (**), p-value ≤0.005 (***) and p-value <0.001 (****).

3. Results

3.1. DNA-GEL forms a spongy three-dimensional matrix in the cell culture medium

We compared the behaviour of DNA-GEL and DNA-NoGEL samples, whose substantial difference resides in the presence, in the DNA-GEL case, of attractive interactions between the NSs.[2] Specifically, DNA-GEL is composed of double-stranded DNA NSs, which are able to bind *via* sticky ends placed on the tip of the NS arms. Conversely, DNA-NoGEL consists of non-interacting NSs (except for the excluded volume or electrostatic repulsion) due to the lack of sticky ends. Hence, at every temperature (below the NS formation temperature T_{NS}), the DNA-NoGEL system is expected to be composed of a ("fluid") solution of freely diffusing DNA NSs, while the DNA-GEL is expected to form a gel below T_g.

We evaluated the DNA-GEL assembly under different conditions mimicking cell cultures by fluorescence microscopy using FITC-conjugated DNA NSs. DNA-GEL and DNA-NoGEL were tested at c = 35 μM and resuspended either in 116 mM NaCl or in a DMEM/Ham's F12 cell culture medium plus 10% FBS (DMEM-FBS). The samples were visualized after 24 h of incubation at T = 37 °C (see Fig. 3A).

When DNA-GEL was suspended in 116 mM NaCl, no structure was observed at microscopic resolution (max ×1000 enlargement). Conversely, DMEM-FBS promoted the formation of a three-dimensional "spongy" structure, showing well-defined pores with a diameter of 10–100 μm, suggesting the formation of a higher-level matrix.

As expected, under all tested conditions, no structure was observed with DNA-NoGEL, which confirms the lack of interactions among the NSs.

We then investigated the behaviour of the DNA-GEL in DMEM-FBS upon temperature variation (see Fig. 3B). We observed that the formation of the "sponge"-like structure was

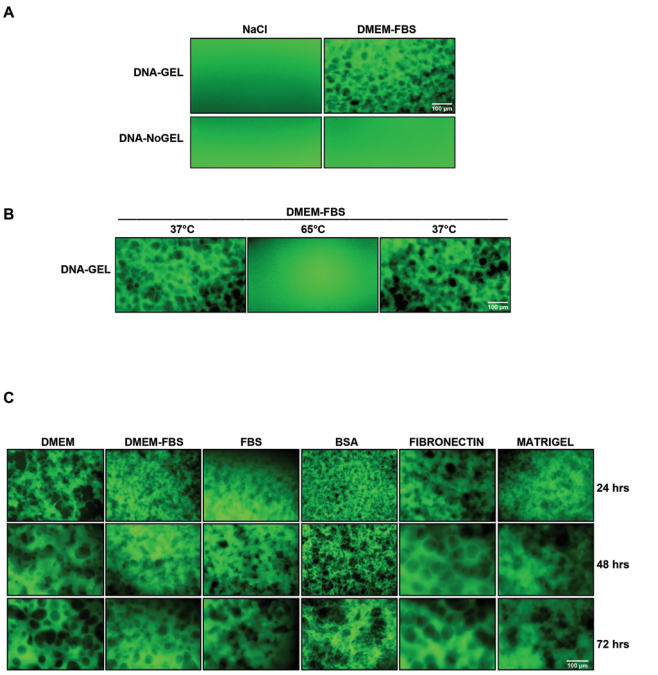

Fig. 3 Three-dimensional macrostructure of DNA-GEL under the cell culture conditions. (A) Fluorescence microscopy images of the DNA-GEL (top) and DNA-NoGEL (bottom) samples (c = 35 μM), prepared using FITC-conjugated NSs and suspended either in 116 mM NaCl (left) or DMEM-FBS (right). Images were obtained with ×10 objective magnification and were acquired after 24 h of incubation at T = 37 °C. (B) Temperature dependence and reversibility of DNA-GEL formation. DNA-GEL (c = 35 μM) was suspended in DMEM-FBS and incubated for 24 h at 37 °C (left), heated at 65 °C for 5 min to unbind the DNA NSs and dissolve the network (center) and incubated again for 24 h at 37 °C (right). (C) Comparison of the DNA-GEL (c = 35 μM) assembly in different protein solutions. From left to right: DMEM, DMEM-FBS and 116 mM NaCl plus 10% FBS (2.5 μg μl^{-1} protein content), 2.5 μg μl^{-1} BSA, 1 μg μl^{-1} fibronectin, or 2.5 μg μl^{-1} Matrigel. Images were acquired after 48 h of incubation at 37 °C.

reversible. In fact, it could be dissolved into a homogeneous suspension after heating for 5 min at T = 65 °C and then reassembled after incubation at T = 37 °C, in agreement with previous investigations.[27,28]

Finally, we studied the type of interactions leading to the assembly of the observed DNA-GEL network under cell culture conditions. The lack of spongy structure formation in 116 mM NaCl and its formation, instead, in DMEM-FBS (at the same temperature and DNA-GEL concentration) suggests an interaction between the NSs of the DNA-GEL and the components of the cell culture medium.

DMEM contains inorganic and organic nutrients, salts, amino acids and sugars. FBS is the main source of macromolecules, such as proteins including BSA – a low molecular weight globular protein – and growth factors. A possible reason for the formation of the macrostructure could be an interaction between DNA-GEL NSs and proteins in the medium. Therefore, we tested the behaviour of DNA-GEL resuspended in different media: DMEM, DMEM-FBS and 116 mM NaCl supplemented with 10% FBS (2.5 μg μl^{-1} of proteins), 2.5 μg μl^{-1} BSA and 1 μg μl^{-1} fibronectin – a high molecular weight glycoprotein able to assemble into fibrils – or 2.5 μg μl^{-1} Matrigel. As shown in Fig. 3C, every kind of protein medium was able to promote the formation of the DNA-GEL "sponge"-like structure. However, clear differences are evident in its morphology, which might be worth investigating more thoroughly in the future.

3.2. BSA interacts with the DNA NSs and changes the gel structure

To better understand the distribution of the proteins with respect to the DNA NSs, we focused on the effect of BSA. In Fig. 4A, we show the fluorescence microscopy images obtained with the samples where Texas Red-conjugated BSA was mixed with either FITC-conjugated DNA-GEL or DNA-NoGEL. When mixed with DNA-GEL, BSA modifies the aggregation behaviour of the DNA NSs. As the concentration of BSA increases – here, from c_{BSA} = 0.5 μg μl^{-1} to 2.5 μg μl^{-1} – the DNA-GEL forms aggregates with different characteristic sizes, from a finely granular structure (at low BSA concentrations) to a coarser one. By comparing the images of the BSA with the ones of the DNA NSs, we can observe that the two species are perfectly colocalized (merge channel). This demonstrates that DNA NSs and BSA effectively interact in the DNA-GEL.

Under our experimental conditions, the system evolves in time towards an equilibrium state *via* nucleation or spinodal decomposition.[29] As a consequence of the underlying phase separation, the system develops concentration inhomogeneities characterized by a typical length scale ξ, as broadly described in section S1 and Fig. S1 and S2 of the ESI.†

Fig. 4B shows how ξ depends on the BSA concentration. We found that the size of the dense and loose regions in the DNA-GEL samples increases with the BSA concentration c_{BSA}. In a phase-separation process, the characteristic length ξ is typically very large and close to the critical temperature and becomes progressively smaller on entering more and more in the coexistence region. This provides a possible thermodynamic interpretation of the observed trend, in which the variation of ξ can be interpreted as a measure of the distance between the experimental temperature and the critical temperature. Based on the analysis of the characteristic size of the density inhomogeneities in the samples shown in Fig. 4A, we conclude that, in this thermodynamic interpretative framework, the macroscopic effect of the addition of BSA is to lower the critical temperature of the DNA NS system. Thus, the phase separation boundaries are affected by the addition of

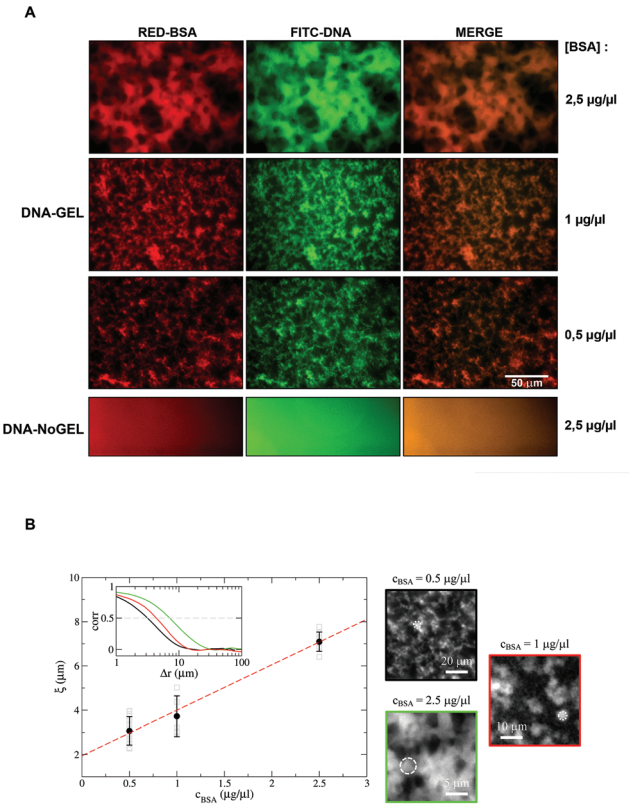

Fig. 4 Changes of the DNA-GEL macrostructure in response to the BSA concentration. (A) Fluorescence microscopy analysis of the FITC-conjugated DNA-GEL (top) and DNA-NoGEL (bottom) at c = 35 μM resuspended in 116 mM NaCl supplemented with Texas Red-conjugated BSA at different concentrations, indicated by the labels. Images were acquired with ×20 objective magnification after 48 h of incubation at 37 °C. From left to right: BSA (red channel), DNA-GEL/DNA-NoGEL (green channel) and merge. (B) Analysis of the density inhomogeneities in the DNA-GEL samples *versus* the BSA concentration. On the left, the main plot shows the characteristic size ξ of the dense and loose regions in the phase separated DNA-GEL samples containing different concentrations of BSA (full dots), after 48 h of incubation at 37 °C. The dashed line is a linear fit to the data. The error bars are evaluated by measuring ξ from different images (data shown with open squares). The inset displays some representative autocorrelation functions measured from the images at the three c_{BSA} investigated: 0.5 μg μl^{-1} (black), 1 μg μl^{-1} (red) and 2.5 μg μl^{-1} (green). The dashed grey line indicates the 0.5 value of the correlation, which was selected to conveniently define ξ. On the right, we show some representative images from the samples at the three different c_{BSA} investigated, indicated by the labels. A dashed circle, with a diameter of 2ξ, is superimposed for comparison.

BSA, consistent with the generic idea that the properties of the solvent (*e.g.*, ionic strength or cosolute concentration) modulate the phase coexistence region.

To explain the formation of a microscopic visible structure, we recall that the interactions between the DNA NSs and BSA are possibly due to hydrophobic and/or hydrogen bond interactions.[30] In the DNA-NoGEL, BSA addition is not able to induce a visible structural organization of the DNA NSs. This suggests that the structures found in the DNA-GEL are not due to aggregation of DNA to the protein structures. The suspension visually behaves as if BSA was not present, with the DNA NSs and BSA uniformly distributed in the sample. Since no effect on the DNA-NoGEL is observed, we speculate that c_{BSA} tunes the binding probability of the DNA sticky ends, generating a network composed of bonded NSs and BSA proteins. The modulation of the binding probability affects the temperature scale of the phase separation, determining an effectively deeper quenching process inside the thermodynamically unstable region upon increasing BSA concentration (see Fig. S3 of the ESI†).

3.3. Interaction between the DNA-GEL matrix and the cells: DNA uptake

The formation of such a microscale structure could be of interest in the biomedical field. Therefore, we tested the behaviour of DNA-GEL as a biocompatible matrix. We investigated the interactions between DNA-GEL and human cells by studying the ability of cells to internalize both DNA-GEL and DNA-NoGEL. We analyzed the DNA uptake in three epithelial cell lines: lung non-small cell adenocarcinoma H1975, renal clear cell carcinoma 786-O and glioblastoma U87MG.

After seeding and adhesion on plates, cells were left untreated (control) or incubated with FITC-conjugated DNA-GEL and DNA-NoGEL (c = 35 μM). The DNA uptake was analyzed by immunofluorescence after 24 and 48 h of incubation (see Fig. 5).

As expected, the untreated control did not reveal any fluorescence signal. The results obtained suggest that our experimental setting was not able to visualize internalized fluorescent DNA in H1975 cells. On the other hand, both 786-O and U87MG cells internalized the DNA-NoGEL as small bodies localized around the nucleus. In Fig. 5, the small arrows indicate the cell nuclei in order to better visualise the localisation of DNA hydrogels. The DNA-GEL, instead, seems to localise as aggregated large bodies in the cytoplasm. These observations suggest that the uptake of DNA is cell type dependent, in agreement with the previously published data.[31]

3.4. Proliferation profiles in the H1975, 786-O and U87MG cells following incubation with DNA-GEL and DNA-NoGEL

Several types of DNA hydrogels have been developed as prototypes for biomedical applications. Despite the considerable work carried out to investigate the structure and the physical properties of gels, very few studies have analysed the effects of DNA hydrogels on the cell behaviour.[3]

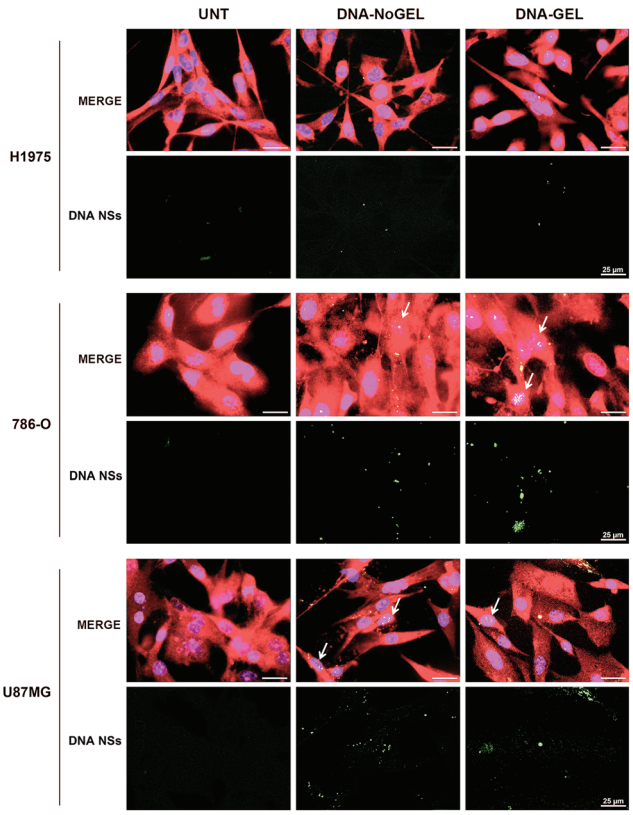

Fig. 5 Cell uptake of DNA-GEL and DNA-NoGEL. Fluorescence microscopy images of (from top to bottom) the H1975, 786-O and U87MG cells after 48 h of incubation, obtained with ×40 objective magnification. DNA-NoGEL (mid column) and DNA-GEL (right column) were prepared using the FITC-conjugated DNA NSs (c = 35 μM, green, shown in the bottom panels for each cell line). The untreated control (UNT) samples are shown on the left. Cells were stained with DAPI (blue) and anti-CD147 (red) in order to visualize their nuclei and membranes. Nuclei are indicated by arrows. The merge with the images displaying the FITC-conjugated DNA NSs are shown in the top panels for each cell line.

We studied the effects produced by DNA-GEL and DNA-NoGEL on three cell lines of different origin and their biological behaviour. In order to evaluate the DNA-GEL biocompatibility and possible toxicity,[32] lung adenocarcinoma H1975, kidney clear cell renal cell carcinoma 786-O and brain glioblastoma U87MG cell lines were tested. After adhesion on plates, cells were left untreated (control) or incubated with DNA-GEL and DNA-NoGEL (c = 35 μM) and their proliferation was followed with time (Fig. 6, left panels).

H1975 cells did not show significant changes upon treatment (Fig. 6A). In contrast, the 786-O (Fig. 6B) and U87MG (Fig. 6C) cells were characterized by a significant reduction of proliferation for both – with DNA-NoGEL and with DNA-GEL. Interestingly, U87MG cells showed a remarkable response to the incubation with both DNA-GEL and DNA-NoGEL, with an almost complete inhibition of growth after 48/72 h. On the other hand, overall, there was no effect of the treatment on cell viability (see section S2 and Fig. S4 of the ESI†).

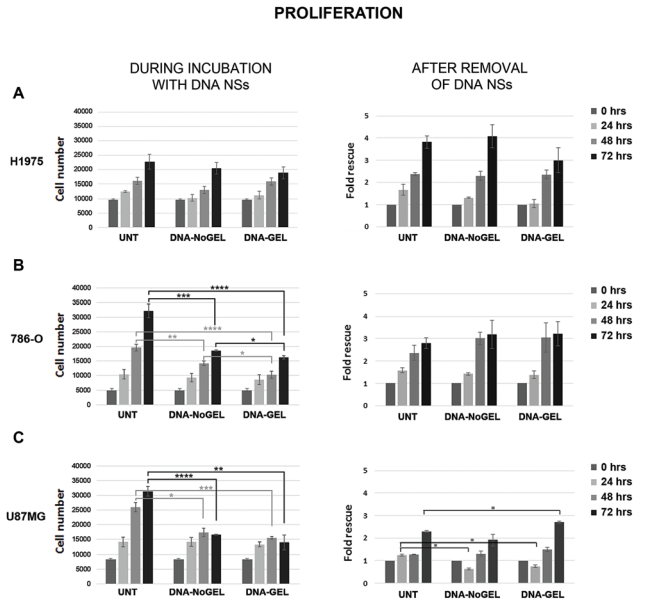

Fig. 6 Cell proliferation of the H1975 (A), 786-O (B) and U87MG cells (C) in the untreated control (UNT) or treated samples with DNA-NoGEL and DNA-GEL (c = 35 μM) at different times, indicated in the legend. The histograms on the left show the number of cells during incubation with the DNA NSs. The histograms on the right show the proliferation fold inductions in cells incubated for 48 h with the DNA NSs and then re-incubated after the removal of the DNA NSs at different times, indicated by the labels. Fold inductions were calculated with respect to the number of cells at time 0 (corresponding to 48 h of treatment with the DNA NSs), at which a value of 1 was arbitrarily assigned.

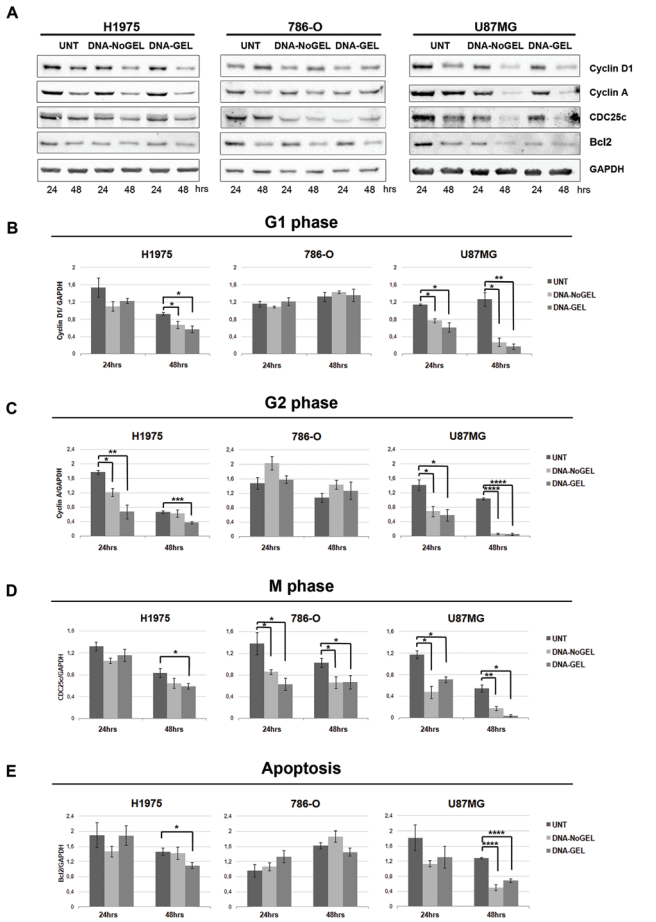

Fig. 7 Effects of DNA-GEL and DNA-NoGEL on cell cycle progression. (A) Western blot analysis of total protein extracts from the H1975, 786-O and U87MG cells, either untreated (UNT) or treated with DNA-NoGEL and DNA-GEL (c = 35 μM) for 24 and 48 h, respectively, as indicated by the labels. Filters were sequentially hybridized with (from top to bottom) Cyclin D1, Cyclin A, CDC25c and Bcl2 antibodies and anti-GAPDH was used for normalization. The histograms (B–E) show the protein amount normalized to the GAPDH control: the G1 phase monitored by anti-Cyclin D1 (B), the G2 phase by anti-Cyclin A (C), mitosis by anti-CDC25c (D) and apoptosis by anti-Bcl2 [33] (E) were evaluated after 24 and 48 h of the treatment.

In order to evaluate whether the decrease of proliferation observed was permanently induced, the DNA NSs were removed from the cells after 48 h of incubation. The cells were washed and incubated in a fresh medium, and proliferation was re-evaluated after 24, 48 and 72 h. The results are shown in Fig. 6 (right panels). The histograms show that full recovery of proliferation was obtained in all the cell lines after the hydrogel removal, suggesting that the incubation with DNA NSs is not toxic.

3.5. Effects on the cell cycle progression of DNA-GEL and DNA-NoGEL in the 786-O, H1975 and U87MG cell lines

Collectively, the previously described results suggest that, during DNA NS incubation, the cells undergo a temporary suspension of cell cycle progression rather than cell death. In order to analyze this hypothesis, we performed western blot analysis to measure the expression of selected cell cycle markers. Total proteins extracted from the cells either left untreated (control) or incubated with DNA-GEL and DNA-NoGEL (c = 35 μM) for 24 and 48 h were analyzed. The expression levels of Cyclin D1 – synthesized during the G1 phase,[34] Cyclin A – mainly expressed in the late G2 phase,[35] CDC25c – expressed at the entry of mitosis[36] and the antiapoptotic protein Bcl2 were tested.

Fig. 7A shows the hybridization of the indicated markers in the three cell lines: lung adenocarcinoma H1975, kidney clear cell renal cell carcinoma 786-O and brain glioblastoma U87MG. The heterogeneity of bands observed was carefully measured and the results are reported in the histograms for each cell cycle phase. In particular, the H1975 and U87MG cells showed a significant reduction of the expression of G1 phase-specific Cyclin D1 (see Fig. 7B) and an even more pronounced reduction of Cyclin A, the G2 marker (see Fig. 7C). In contrast, no effects were found in the 786-O cells. Moreover, the cell lines showed a striking reduction of the pre-mitotic marker CDC25c (see Fig. 7D), indicating a defect in the mitosis entry.

Overall, our results suggest that there is a general inhibition of the cell cycle progression in all the cell lines tested. Remarkably, the comparative analysis of the data shown in Fig. 7 indicates that the most prominent effect was induced by

the treatment of U87MG cell lines, in which both DNA-GEL and DNA-NoGEL incubation caused a dramatic inhibition of G1, G2 and M phase entry, further associated with a contemporary induction of apoptosis, as demonstrated by the dramatic down-regulation of the antiapoptotic Bcl2 protein (see Fig. 7E).

3.6. DNA-GEL and DNA-NoGEL reduce the migration of the 786-O, H1975 and U87MG cell lines

The acquisition of invasive and metastatic qualities is a fundamental hallmark in the light of malignant progression.[37] To understand the possible effects of DNA NS incubation on the migration and invasiveness of 786-O, U87MG and H1975 cell lines, we performed the wound healing assay on cells incubated for 24 h with DNA-GEL and DNA-NoGEL (c = 35 μM). The results obtained are shown in Fig. 8A.

The mobility observed in the different cell lines reflects the intrinsic adhesion and motility features of each type of cell line.[38] It is known, in fact, that the epithelial-derived H1975 cell line is far less capable of strongly adhering to the surface and this can interfere with gap filling.[39] Accordingly, incubation of H1975 with DNA-NoGEL did not show a significant effect and overall the wound filling was similar to that of the untreated control. On the other hand, in the presence of DNA-GEL, cells displayed a poorer wound healing capacity. Both DNA-NoGEL and DNA-GEL induced a stronger inhibitory effect on 786-O cells with respect to the control. However, in the presence of DNA-GEL, the wound persisted unfilled after 48 h from the scratch. In U87MG, wound healing displayed a similar trend of ccRCC 786-O cells, as the migration was decreased both by DNA-NoGEL and – more efficiently – by DNA-GEL. In the table shown in Fig. 8B, the filled area measured after 48 h clearly showed the stronger inhibition produced by the incubation with DNA-GEL. Likely, the impairment of migration described could be related to a physical restraint due to the higher viscosity produced by the presence of the DNA NSs.

To understand whether the inhibitory effects described were reversible, the wound healing experiment was performed after the removal of the DNA NSs. Cells were treated with DNA-GEL and DNA-NoGEL for 48 h, washed several times to remove residual DNA NSs and then scratched.

As shown in Fig. 8C, the removal of DNA NSs led to the full rescue of migration in the 786-O and U87MG cell lines, indicating the complete recovery of the migration ability of the original cell line. Finally, to assess whether the presence of DNA NSs might interfere with early and intrinsic cell motility, we performed single cell tracking in a fixed area at different times and analyzed the mean square displacement (MSD), as shown in Fig. 8D. The results show that motility of H1975 cells was slightly reduced by DNA-GEL, while their behaviour in the presence of DNA-NoGEL was not affected. The DNA NSs reduced the motility of 786-O cells, with a far more drastic effect in the DNA-GEL sample. The motility of U87MG cells was drastically reduced in both DNA-GEL and DNA-NoGEL samples. Based on the motility results, we can assume that DNA-NoGEL and – even more – DNA-GEL affect the cellular motility soon after scratching.

4. Discussion

In this study, we have tested DNA hydrogels composed of DNA tetravalent NSs with protruding interacting sticky ends. The possibility to choose the nucleotide sequence and length of the protruding ends of the arms allows to obtain gels with the desired melting temperature and to modulate their behaviour, as reviewed by Lattuada *et al.*[3] We found that the macrostructure of DNA-GEL is affected by the protein concentration and physiological temperature (37 °C), which cause a thermodynamic instability and an inhomogeneous spatial distribution of DNA NSs, with regions with a higher or lower concentration of the NSs. The DNA-GEL macrostructure is an important feature also in light of future biological applications for the delivery of molecules *in vivo*.

4.1. The macroscopic structure of DNA-GEL under cell culture conditions

In order to understand the three-dimensional structure of the gel-forming NSs under cell culture conditions – whose features are relevant for biological and cellular purposes – we analyzed, at the microscopic scale, the DNA-GEL macrostructure in different solvent environments (most of them of biological relevance).

We demonstrated that the DNA-GEL structure changes with temperature and protein concentration. The presence of dense gel regions, together with more diluted ones (composed of freely diffusing NSs at a low concentration), produces a typical "sponge"-like structure. As exhaustively explained in section S1 of the ESI,† this behaviour is generated by a phase separation at 37 °C characterized by a typical length scale ξ, which responds to changes in the solvent conditions (including the presence of proteins). Specifically, the size of the dense and loose regions that characterize the overall macrostructure of the DNA-GEL increases with the protein concentration. On the other hand, no macrostructure was observed with the non-interacting NSs in the DNA-NoGEL, as expected.

The typical "spongy" gel structure formed by DNA-GEL under the cell culture conditions can be conveniently applied and implemented for the delivery of different kinds of compounds or active molecules.

4.2. H1975, 786-O and U87MG cells show specific responses to incubation with DNA-GEL and DNA-NoGEL

The aim of this study was to provide an extensive analysis of how different cell lines respond to incubation with DNA hydrogels. While there is a wide literature describing the physical properties of different types of DNA hydrogels,[2,6,11,40–43] there is a lack of information on how different cells respond to the incubation with gel-forming DNA-based nanomaterials. We have analyzed three cell lines representing human aggressive neoplasms: lung adenocarcinoma H1975,[44,45] kidney clear cell

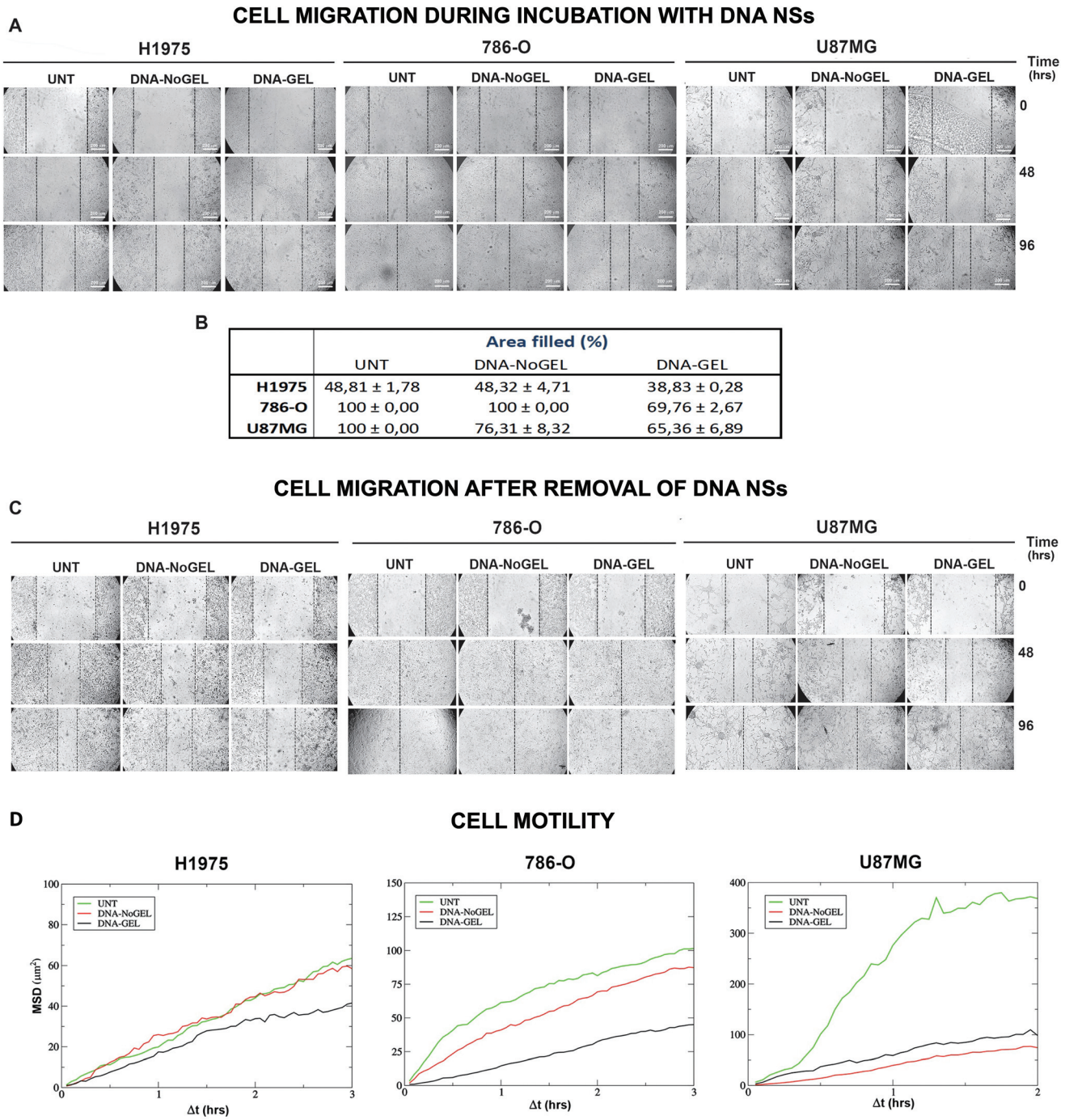

Fig. 8 Effects of DNA-GEL and DNA-NoGEL on cell migration. (A) A wound healing assay was performed on (from left to right) the H1975, 786-O and U87MG cell lines. Cells were incubated for 24 h with DNA-GEL and DNA-NoGEL (c = 35 μM) and cell migration was followed at different times, indicated by the labels. For each cell line, the untreated control (UNT) is shown on the left. (B) The percentage of the wound filling area, calculated as described in section 2.8. The results obtained after 48 h are shown in the table. (C) The recovery was evaluated in the cells incubated for 48 h with DNA-GEL and DNA-NoGEL (c = 35 μM) and followed at different times (indicated by the labels) after the DNA NS removal. The untreated control is shown on the left for each cell line. (D) The plots show the mean square displacement of the H1975, 786-0 and U87MG cells, measured near the wound, over 5 h after the scratch.

carcinoma 786-O[46,47] and brain glioblastoma U87MG.[18,48,49] In particular, we studied the response of these cell lines by analyzing different biological effects induced by incubation with DNA hydrogels.

In this study, we found that the response of different cell lines is specific. However, the robustness of the effects was quantitatively different. Indeed, we observed that each cell line shows different uptake of DNA-GEL and DNA-NoGEL. Also, cell

proliferation in response to incubation with DNA-GEL and DNA-NoGEL was different and was inhibited in 786-O cells and even more in U87MG cells. The analysis of the cell cycle progression during the incubation of cells with DNA-GEL followed by the expression of phase-specific markers indicated, overall, that the cells showed a block of proliferation. Indeed, the 786-O cells were delayed at the mitosis entry, whereas the H1975 cells and even more the U87MG cells showed delay in G1/G2 transition and mitosis delay, thus showing decrease of the antiapoptotic factor Bcl2.[50] Finally, the analysis of cell motility and migration upon incubation with DNA-GEL and DNA-NoGEL suggested that the higher viscosity of the gel regions may represent an environmental constraint for the cells, a sort of a cage inhibiting their free movement.

It is worth noting that the data obtained with the U87MG cell line show that these cells were particularly affected by the treatment with DNA-GEL, displaying a clear decrease of proliferation and migration.

Pinning down the reduction of motility observed to an increase of viscosity of the gel – even if consistent with previous studies indicating the increase of gel viscosity with respect to the fluid phase[51,52] – could be, of course, an oversimplification. We cannot exclude other effects, such as possible specific interactions between the gel matrix and the cells and/or the specific ability of the cells to interact with the hydrogel pores and surfaces. Further studies are needed in order to resolve such effects in a more thorough way. Possible improvements of the analysis could resort to combined systematic rheological tests and measurements of the motility *via* a "two-point" MSD, which could help sort out the effects due to material inhomogeneities.[53]

It is interesting to note that proliferation and cell cycle did not show significant differences upon treatment with DNA-NoGEL with respect to DNA-GEL. These results suggest that there are no qualitative differences in the effects induced by the non-interacting DNA NSs or interacting (gel-forming) NSs. On the other hand, we found that the DNA-GEL is more effective in the inhibition of cell migration compared to the DNA-NoGEL. This evidence suggests that the network of NSs produces a sort of cage which is able to hamper the migration and cellular movements. Overall, the results we collected suggest that – in a not so distant future – DNA-GEL could be productively employed in next generation protocols for at least two reasons: (i) the possibility to obtain a DNA gel that can easily incorporate the desired drugs or macromolecules (*e.g.*, miRNAs), which are effective inside the tissues, and (ii) the possibility to wrap a selected tissue or tumor with a precast desired DNA-GEL able to counteract cell migration as a novel tool for a slower and more prolonged diffusion of bioactive molecules into the tissues.

In our opinion, these results appear to be promising: glioblastoma is a highly lethal tumor, which is generally unresponsive to antiproliferative agents and which usually foreshadows a poor prognosis despite aggressive clinical treatment.[54] Needless to say, it certainly deserves further investigations, in order to understand if the use of DNA-GEL may represent an efficient strategy to counteract the diffuse invasion of glioblastoma cells. In particular, the G2/M inhibition on glioblastoma might be used with other G2/M inhibitors proven to have synergistic effects with the standard temozolomide and radiation glioblastoma therapy.[54,55]

4.3. DNA-GEL and DNA-NoGEL do not induce toxic effects on cells

The main observation is that the treatment of cells with DNA-GEL and DNA-NoGEL does not induce cell death. Accordingly, among nanomaterials, DNA-GEL can be considered as a good candidate for the delivery and administration of different molecules and compounds.

Interestingly, we found different responses of the three cell lines to the application of DNA-GEL itself, indicating a specificity in the response. It was reported that spontaneous uptake of double-stranded DNA occurs and is a cell-type dependent process.[56] Additionally, oligonucleotides – either as free molecules or conjugated with specific molecules or conjugated with nanoparticles – usually enter cells *via* endocytosis, but they have to traverse multiple intracellular pathways and be directed to distinct subcellular compartments.[57–59] Internalization of DNA-GEL and recovery of growth after DNA-GEL removal indicate a lack of toxicity of this treatment on the cell lines tested. Therefore, on the basis of these experimental findings, we can propose novel protocols for the *in situ* applications of the DNA-GEL in a specific tissue, representing a non-toxic nanomaterial able to concentrate any desired deliverable molecules that can be slowly released inside tissues.

5. Conclusions

We have demonstrated that DNA-based hydrogels composed of interacting four-armed DNA NSs can be used for the treatment of human cell cultures, inducing type-specific cell responses without detrimental impact on cell survival.

We have shown the DNA-GEL structure at the cell-size scale obtained under cell culture conditions and how it is influenced by factors and proteins in the medium. The peculiarity of this structure depends on the coexistence of dense (gel) and loose regions generated by an underlying phase separation process. These observations could be useful for future applications.

Indeed, the data on cell migration upon DNA-GEL treatment suggest that the macrostructure of DNA-GEL surrounds the cells, representing a highly viscous environment that hinders their free movement.

Experimental results also demonstrate that DNA-GEL is biocompatible, non-toxic and well tolerated and all cells survive the treatment.

In addition, we show that the different cell lines tested showed specific responses to the treatment with more or less pronounced effects: in particular, clear cell renal cell carci-

noma 786-O and glioblastoma U87MG cells showed more marked effects than lung adenocarcinoma H1975 cells.

We also report that cell cycle progression is halted by DNA-GEL treatment and that cells are able to resume growth some time after the removal of the DNA-GEL. This result is particularly interesting in light of the possible delivery of bioactive molecules and compounds in tissues.

Author contributions

A. S., F. S. and P. F. conceptualized the study and supervised the project. M. L., E. L., D. C. and L. S. performed the experiments. P. F., A. S., F. S. and A. V. contributed to the final data interpretation. M. L., E. L., D. C., L. S., F. S., P. F. and A. S. contributed to writing the original draft of the manuscript. M. L., E. L. and L. S. edited the final version of the manuscript, which was finally reviewed by all the authors.

Conflicts of interest

There are no conflicts to declare.

Acknowledgements

This work was supported by the Lazio-Innova project DNA-GEL (grant no. 85857-0051-0085) from Regione Lazio, with postdoc grants to E. L. and M. L., and grants RM11916B85524428 and RM11816430E896B2. F. S. and E. L. acknowledge support from MIUR-PRIN (grant no. 2017Z55KCW). We thank M. Giubettini and CrestOptics S.p.A. for the microscopy images.

References

1 N. C. Seeman, *Nature*, 2003, **421**, 427–431.
2 S. Biffi, R. Cerbino, F. Bomboi, E. M. Paraboschi, R. Asselta, F. Sciortino and T. Bellini, *Proc. Natl. Acad. Sci. U. S. A.*, 2013, **110**, 15633–15637.
3 E. Lattuada, M. Leo, D. Caprara, L. Salvatori, A. Stoppacciaro, F. Sciortino and P. Filetici, *Front. Pharmacol.*, 2020, **11**, 1345.
4 Y. Ke, L. L. Ong, W. M. Shih and P. Yin, *Science*, 2012, **338**, 1177–1183.
5 F. Bomboi, F. Romano, M. Leo, J. Fernandez-Castanon, R. Cerbino, T. Bellini, F. Bordi, P. Filetici and F. Sciortino, *Nat. Commun.*, 2016, **7**, 1–6.
6 M. Nishikawa, K. Ogawa, Y. Umeki, K. Mohri, Y. Kawasaki, H. Watanabe, N. Takahashi, E. Kusuki, R. Takahashi, Y. Takahashi, *et al.*, *J. Controlled Release*, 2014, **180**, 25–32.
7 Y. Ishii-Mizuno, Y. Umeki, Y. Onuki, H. Watanabe, Y. Takahashi, Y. Takakura and M. Nishikawa, *Int. J. Pharm.*, 2017, **516**, 392–400.
8 Y. Umeki, M. Saito, Y. Takahashi, Y. Takakura and M. Nishikawa, *Adv. Healthcare Mater.*, 2017, **6**, 1700355.
9 Y. Shao, Z.-Y. Sun, Y. Wang, B.-D. Zhang, D. Liu and Y.-M. Li, *ACS Appl. Mater. Interfaces*, 2018, **10**, 9310–9314.
10 F. Komura, K. Okuzumi, Y. Takahashi, Y. Takakura and M. Nishikawa, *Molecules*, 2020, **25**, 728.
11 S. H. Um, J. B. Lee, N. Park, S. Y. Kwon, C. C. Umbach and D. Luo, *Nat. Mater.*, 2006, **5**, 797–801.
12 M. Nishikawa, Y. Mizuno, K. Mohri, N. Matsuoka, S. Rattanakiat, Y. Takahashi, H. Funabashi, D. Luo and Y. Takakura, *Biomaterials*, 2011, **32**, 488–494.
13 J. Song, K. Im, S. Hwang, J. Hur, J. Nam, G.-O. Ahn, S. Hwang, S. Kim and N. Park, *Nanoscale*, 2015, **7**, 9433–9437.
14 C. Liu, J. Han, Y. Pei and J. Du, *Appl. Sci.*, 2018, **8**, 1941.
15 H. Wei, Z. Zhao, Y. Wang, J. Zou, Q. Lin and Y. Duan, *ACS Appl. Mater. Interfaces*, 2019, **11**, 46479–46489.
16 L. Yue, S. Wang, V. Wulf and I. Willner, *Nat. Commun.*, 2019, **10**, 1–10.
17 F. Bomboi, S. Biffi, R. Cerbino, T. Bellini, F. Bordi and F. Sciortino, *Eur. Phys. J. E*, 2015, **38**, 1–8.
18 W. Diao, X. Tong, C. Yang, F. Zhang, C. Bao, H. Chen, L. Liu, M. Li, F. Ye, Q. Fan, *et al.*, *Sci. Rep.*, 2019, **9**, 1–9.
19 M. G. Noro and D. Frenkel, *J. Chem. Phys.*, 2000, **113**, 2941–2944.
20 G. Foffi and F. Sciortino, *J. Phys. Chem. B*, 2007, **111**, 9702–9705.
21 M. S. Wertheim, *J. Stat. Phys.*, 1984, **35**, 35–47.
22 M. S. Wertheim, *J. Stat. Phys.*, 1986, **42**, 459–476.
23 J. SantaLucia, *Proc. Natl. Acad. Sci. U. S. A.*, 1998, **95**, 1460–1465.
24 J. N. Zadeh, C. D. Steenberg, J. S. Bois, B. R. Wolfe, M. B. Pierce, A. R. Khan, R. M. Dirks and N. A. Pierce, *J. Comput. Chem.*, 2011, **32**, 170–173.
25 L. G. Rodriguez, X. Wu and J.-L. Guan, *Cell migration*, Springer, 2005, pp. 23–29.
26 J.-Y. Tinevez, N. Perry, J. Schindelin, G. M. Hoopes, G. D. Reynolds, E. Laplantine, S. Y. Bednarek, S. L. Shorte and K. W. Eliceiri, *Methods*, 2017, **115**, 80–90.
27 S. Biffi, R. Cerbino, G. Nava, F. Bomboi, F. Sciortino and T. Bellini, *Soft Matter*, 2015, **11**, 3132–3138.
28 J. Fernandez-Castanon, F. Bomboi, L. Rovigatti, M. Zanatta, A. Paciaroni, L. Comez, L. Porcar, C. J. Jafta, G. C. Fadda, T. Bellini, *et al.*, *J. Chem. Phys.*, 2016, **145**, 084910.
29 R. A. L. Jones, *Soft Condensed Matter*, OUP Oxford, 2002.
30 N. M. Luscombe, R. A. Laskowski and J. M. Thornton, *Nucleic Acids Res.*, 2001, **29**, 2860–2874.
31 R. L. Juliano and K. Carver, *Adv. Drug Delivery Rev.*, 2015, **87**, 35–45.
32 A. Sukhanova, S. Bozrova, P. Sokolov, M. Berestovoy, A. Karaulov and I. Nabiev, *Nanoscale Res. Lett.*, 2018, **13**, 1–21.
33 P. E. Czabotar, G. Lessene, A. Strasser and J. M. Adams, *Nat. Rev. Mol. Cell Biol.*, 2014, **15**, 49–63.
34 M. Fu, C. Wang, Z. Li, T. Sakamaki and R. G. Pestell, *Endocrinology*, 2004, **145**, 5439–5447.
35 C. H. Yam, T. K. Fung and R. Y. C. Poon, *Cell. Mol. Life Sci.*, 2002, **59**, 1317–1326.

36 K. Liu, M. Zheng, R. Lu, J. Du, Q. Zhao, Z. Li, Y. Li and S. Zhang, *Cancer Cell Int.*, 2020, **20**, 1–16.
37 T. Brabletz, A. Jung, S. Spaderna, F. Hlubek and T. Kirchner, *Nat. Rev. Cancer*, 2005, **5**, 744–749.
38 H. Läubli and L. Borsig, *Front. Immunol.*, 2019, **10**, 2120.
39 D. Stichel, A. M. Middleton, B. F. Müller, S. Depner, U. Klingmüller, K. Breuhahn and F. Matthäus, *npj Syst. Biol. Appl.*, 2017, **3**, 1–10.
40 Q. Hu, H. Li, L. Wang, H. Gu and C. Fan, *Chem. Rev.*, 2018, **119**, 6459–6506.
41 E. Cheng, Y. Xing, P. Chen, Y. Yang, Y. Sun, D. Zhou, L. Xu, Q. Fan and D. Liu, *Angew. Chem., Int. Ed.*, 2009, **48**, 7660–7663.
42 Y. Murakami and M. Maeda, *Biomacromolecules*, 2005, **6**, 2927–2929.
43 H. Kang, H. Liu, X. Zhang, J. Yan, Z. Zhu, L. Peng, H. Yang, Y. Kim and W. Tan, *Langmuir*, 2011, **27**, 399–408.
44 A. Bhattacharjee, W. G. Richards, J. Staunton, C. Li, S. Monti, P. Vasa, C. Ladd, J. Beheshti, R. Bueno, M. Gillette, *et al.*, *Proc. Natl. Acad. Sci. U. S. A.*, 2001, **98**, 13790–13795.
45 S. Usui, Y. Minami, T. Shiozawa, S. Iyama, K. Satomi, S. Sakashita, Y. Sato and M. Noguchi, *Lung Cancer*, 2013, **82**, 407–412.
46 J. J. Hsieh, M. P. Purdue, S. Signoretti, C. Swanton, L. Albiges, M. Schmidinger, D. Y. Heng, J. Larkin and V. Ficarra, *Nat. Rev. Dis. Primers*, 2017, **3**, 1–19.
47 J. Xu, Y. Liu, J. Liu, Y. Shou, Z. Xiong, H. Xiong, T. Xu, Q. Wang, D. Liu, H. Liang, *et al.*, *Front. Oncol.*, 2021, **11**, 659208.
48 V. A. Cuddapah, S. Robel, S. Watkins and H. Sontheimer, *Nat. Rev. Neurosci.*, 2014, **15**, 455–465.
49 J. H. Hwang, C. A. Smith, B. Salhia and J. T. Rutka, *Neoplasia*, 2008, **10**, 149–159.
50 Y. Tsujimoto, *Genes Cells*, 1998, **3**, 697–707.
51 J. Fernandez-Castanon, S. Bianchi, F. Saglimbeni, R. Di Leonardo and F. Sciortino, *Soft Matter*, 2018, **14**, 6431–6438.
52 Z. Xing, A. Caciagli, T. Cao, I. Stoev, M. Zupkauskas, T. O'Neill, T. Wenzel, R. Lamboll, D. Liu and E. Eiser, *Proc. Natl. Acad. Sci. U. S. A.*, 2018, **115**, 8137–8142.
53 J. C. Crocker, M. T. Valentine, E. R. Weeks, T. Gisler, P. D. Kaplan, A. G. Yodh and D. A. Weitz, *Phys. Rev. Lett.*, 2000, **85**, 888.
54 R. Stupp, W. P. Mason, M. J. van den Bent, M. Weller, B. Fisher, M. J. Taphoorn, K. Belanger, A. A. Brandes, C. Marosi, U. Bogdahn, J. Curschmann, R. C. Janzer, S. K. Ludwin, T. Gorlia, A. Allgeier, D. Lacombe, J. G. Cairncross, E. Eisenhauer and R. O. Mirimanoff, *N. Engl. J. Med.*, 2005, **352**, 987–996.
55 A. M. Castro-Gamero, J. A. Pezuk, M. S. Brassesco and L. G. Tone, *Cancer Biol. Med.*, 2018, **15**, 354.
56 M. J. Lehmann and G. Sczakiel, *Gene Ther.*, 2005, **12**, 446–451.
57 R. L. Juliano, *Nucleic Acids Res.*, 2016, **44**, 6518–6548.
58 C. J. Choi, L. Hao, S. P. Narayan, E. Auyeung and C. A. Mirkin, *Proc. Natl. Acad. Sci. U. S. A.*, 2013, **110**, 7625–7630.
59 D. Mumcuoglu, M. Sardan Ekiz, G. Gunay, T. Tekinay, A. B. Tekinay and M. O. Guler, *ACS Appl. Mater. Interfaces*, 2016, **8**, 11280–11287.